

# **Bond Behaviour and Sustainability of Fibre Reinforced Cementitious Matrix Composites applied to Masonry Elements**

**J.H. Gonzalez<sup>1</sup>, F. Faleschini<sup>1</sup>, T. D'Antino<sup>2</sup> and C. Pellegrino<sup>1</sup>**

<sup>1</sup>**Civil, Architectural and Environmental Engineering Department  
University of Padua, Italy**

<sup>2</sup>**Department of Civil Engineering  
University of Patras, Greece**

## **Abstract**

Fibre-reinforced polymers (FRP) have shown to be an effective solution for retrofitting and strengthening of existing masonry structures, although some drawbacks related with the use of organic resins have been found. A newly developed alternative to FRP, known as fibre reinforced cementitious matrix (FRCM) composites, may overcome the drawbacks. This paper provides a better insight into the bond behaviour of FRCM when applied to masonry substrates and highlights possible differences with the behaviour of FRP composites by means of push-pull single-lap direct-shear tests for two types of fibres (glass and basalt). Additionally, the sustainability of this strengthening system was evaluated by means of a life cycle assessment (LCA). The experimental data suggests that the effective bond length for basalt FRCM composites is lower than 260 mm and that for basalt and glass composites the initial response is highly dependent on the elastic behaviour of the fibres. The FRCM system provides environmental benefits in all the analysed categories with respect to the reference FRP technique, based on the analysis performed.

**Keywords:** fibre reinforced cementitious matrix, masonry, bond behaviour, single-lap direct-shear test, glass, basalt, sustainability, life cycle assessment.

## **1 Introduction**

Masonry structures, either historical or more recently built, usually require interventions to meet new or increased loads, achieve new requirements proposed by current standards or guarantee their capacity to withstand seismic actions [1]. In past years, the use of fibre-reinforced polymers (FRP) composites have shown to be an efficient alternative for the retrofitting and strengthening of existing masonry structures mainly due to its low invasiveness, high strength, and ease of application. Nevertheless, the use of organic resins presents some drawbacks such as poor

behaviour at temperatures close or above the glass transition temperature, poor compatibility with the substrate, inability to apply the system on wet surfaces or at low temperatures, and inconvenience to carry out post-earthquake assessment of damaged structures [2]. A newly developed alternative to the use of FRP composites that may overcome the aforementioned limitations is represented by fibre reinforced cementitious matrix (FRCM) composites, which are comprised of high strength fibres embedded within an inorganic matrix.. The literature in the subject is still scarce and an important effort is still needed in order to fully understand behaviour and applicability of FRCM composites.

Among the properties that need to be investigated, the bond behaviour appears to play a key role in the overall performance of the composite system [3]. Recent experimental studies have shown that bond between the FRCM composites and masonry substrates presents differences with respect to the FRP-masonry and FRP-concrete bond behaviour. Indeed, in most of the cases, the debonding surface of FRP composites applied on different substrates is characterized by detachment of a thin layer of the support material [4, 5], while in case of FRCM materials a different debonding mechanisms involving the fibres/matrix interface has been observed [4, 5, 6].

This paper intends to obtain a better insight of bond behaviour of FRCM composites when applied on masonry substrates and highlight possible differences with the more known behaviour of FRP composites. In order to do so, push-pull single-lap direct-shear tests were performed. Two different types of fibres were used (glass and basalt).

Furthermore, the sustainability of this strengthening system was evaluated by means of a life cycle assessment (LCA) approach. The decision-making process of a retrofit or strengthening operation should in fact take into account also sustainability purposes, leading to a best option which optimizes a range of problems involving energetic, economic, technical, social, regulations, and lastly environmental aspects. Accordingly, glass and basalt fibres were analysed, and the environmental impacts of the retrofit operations using FRCM and FRP systems were evaluated. The final aim of this work is to provide practitioners and researchers a proper quantification of the sustainability improvements gained by the use of cementitious matrix in place of polymers, and highlight the differences between different types of fibres for FRCM composites.

## **2 FRCM bond behaviour**

As defined by Cheng and Teng [7], the effective bond length ( $l_e$ ) is the length beyond which an extension of the bond length cannot increase the bond strength. In order to avoid undesirable debonding failures, the assessment of the effective bond length is crucial for proper designing FRP or FRCM strengthened structures and to determine the actual bond strength.

Research carried out on FRP applied on masonry substrates has shown that a load versus displacement curve follows a linear behaviour, followed by a nonlinear

branch after which the stress stabilizes and remains basically constant until failure [8]. Local drops in the experimental response, due to the presence of mortar joints, have been reported [9]. Failure is reached in most of the cases due to debonding.

However, the knowledge about the performance of FRCM on masonry substrates is still limited. ACI549.4R-13 [10] proposes a constant value of 15 cm for effective bond length, regardless of the quality of the matrix, type of fibre, and type of substrate and no explanation about the research background behind the selection of this value is provided. In addition, some contradictory results can be found on the research carried out in the topic, although debonding at the matrix-fibre interface instead of the matrix-concrete interface has been generally reported.

D'Ambrisi et al [1], using double shear tests, reported a value of the effective bond length slightly lower than 100 mm for carbon FRCM-concrete joints. The load responses they obtained resemble the idealized curve put together by D'Antino et al [11] for PBO FRCM-concrete joints, shown in Figure 1. As in case of FRP composites, the applied load increases linearly until a point after which the load response becomes non-linear and the debonding load  $P_{deb}$  is reached. However, due to the presence of friction (interlocking) between fibre filaments and between fibres and matrix, which was not observed in case of FRP-concrete joints,  $P$  increases from  $P_{deb}$  due to the shifting of the stress transfer mechanism along the composite bonded length towards the free end. Assuming a bonded length longer than  $l_e$ , the peak load,  $P^*$ , is attained when the stress transfer mechanism reached the free end and the length along which debonding is not occurred yet, named residual bonded length, is equal to  $l_e$ . After this point, the applied load decreases with increasing global slip until the fibres are completely debonded and a constant applied load  $P_f$ , due only to friction, remains.

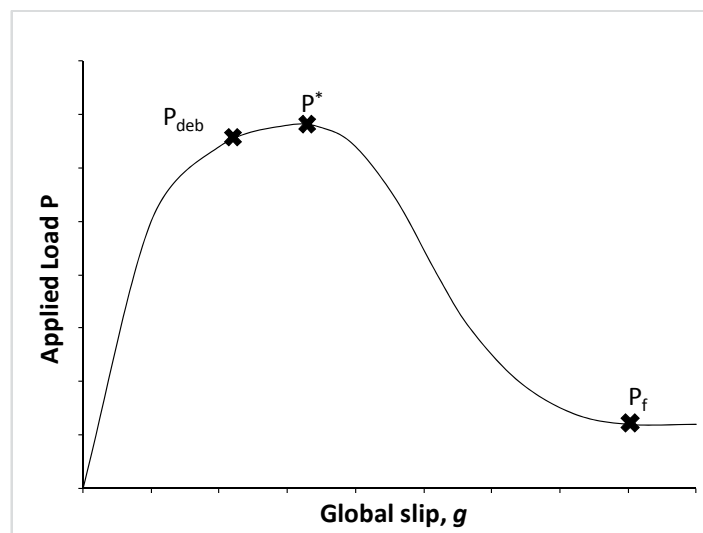


Figure 1: Idealized applied load – global slip response [11]

However, load responses obtained by Carozzi and Poggi [6] using double shear tests reported a different trend that can be described as quasi-linear until peak load

followed by a sudden failure. They also observed good adhesion between the masonry substrate and the FRCM system, slippage phenomena at the matrix-fibre interface depending on the type of fibre, and collapse caused by tensile failure of the bundles generally outside the bonded length. Bonded lengths, for the different type of fibres used in the study (carbon, glass, PBO) ranged from 100 to 150 mm, approximately,

### 3 Experimental campaign

#### 3.1 Materials

Basalt and glass fibres were employed in the experimental campaign. The basalt fibres were comprised of fibre bundles spaced at 25 mm in the longitudinal and transversal direction with an overall weight of 350 g/m<sup>2</sup>. Glass fibres were bundled with a spaced of 25 mm in perpendicular directions and with an overall weight of 250 g/m<sup>2</sup>. The areas are of a single fibre bundle ( $A_b$ ) of basalt and glass fibre, as reported by the manufacturer, was 1.45 mm<sup>2</sup> and 1.25 mm<sup>2</sup>, respectively. Three specimens, comprised of one single bundle 500 mm long for each type of fibre, were tested in tension (Figure 2a). Two aluminium plates were epoxy bonded at the end of each bundle to avoid slippage at the machine clamps. The tensile tests were conducted in displacement control at rate of 0.5 mm/min following ASTM D3039 [12] and an extensometer with base length 50 mm was applied in the middle of the specimens to measure the strain. The results found for each specimen are listed in Table 1 while the stress–strain curves obtained for both fibres are plotted in Figure 2b.

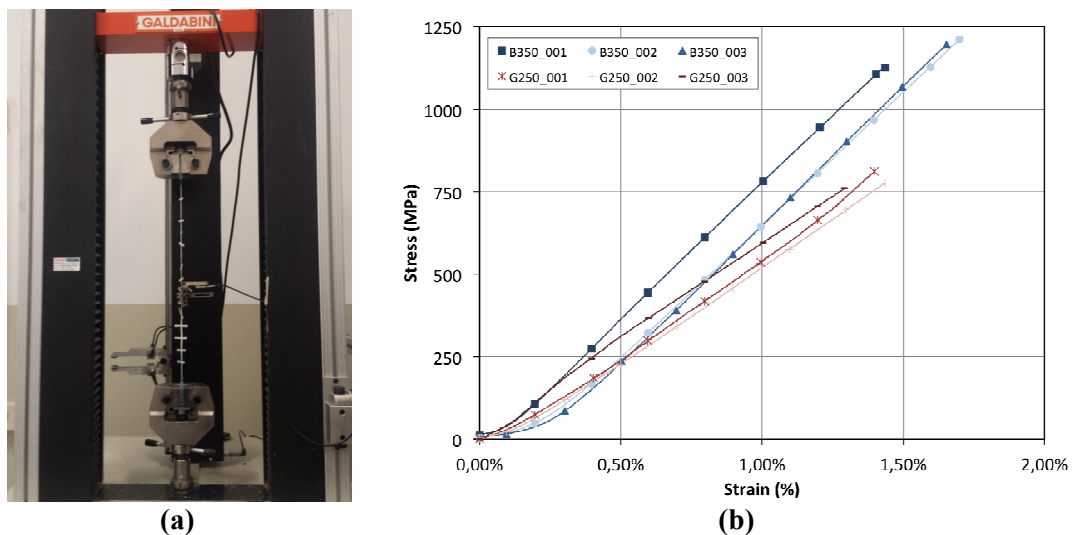


Figure 2: (a) Photo of tensile test. (b) Stress-strain relation of basalt and glass fibres

Specimen	Tensile Peak Load (kN)	Average Tensile Peak Load (kN)	Tensile Stress (MPa)	Average Tensile Stress (MPa)	COV
<b>BASALT FIBRES</b>					
B350_001	1.63	1.71	1126	1177	0.039
B350_002	1.76		1211		
B350_003	1.73		1196		
<b>GLASS FIBRES</b>					
G250_001	1.01	0.99	811	782	0.034
G250_002	1.01		776		
G250_003	0.95		759		

Table 1: Fibre tensile tests results

Two batches of the same matrix, named matrix L, were used at different times to cast the FRCM. Three 40x40x160 mm samples for each batch of matrix were tested on the same day the corresponding direct-shear tests were carried out, according to UNI EN 1015-11 [13]. The first batch had an average flexural strength,  $f_{flex}$ , and average compressive strength,  $r_{cm}$ , equal to 4.79 MPa (CoV= 0.06) and 16.08 MPa (CoV=0.027), respectively. The second batch had  $f_{flex}$ =5.59 MPa (CoV=0.11) and  $r_{cm}$ =16.98 MPa (CoV=0.035).

### 3.2 Single-lap direct-shear test

The bond behaviour of basalt and glass FRCM-masonry specimens is investigated by means of 20 push-pull single lap tests. The substrate was manufactured using “San Marco Rosso Vivo A6R55W” bricks with compressive strength of 20 N/mm<sup>2</sup>, with the geometry shown in Figure 3. A strip of FRCM composite, comprised of one layer of fibre net embedded within two 5 mm thick matrix layers, was applied on the masonry substrate. The bonded width of both FRCM composites,  $b_l$ =75 mm, was designed to include three longitudinal fibre bundles and to leave a distance of half the net spacing between the matrix edge and the external fibre bundle.

In order to study the bond behaviour of FRCM-masonry joints, three different bonded lengths were employed, namely, 100 mm, 200 mm, and 260 mm.

Specimens were named following the notation MS\_FMK\_X\_Y\_Z, where F=fibre employed (B=Basalt, G=glass), M=matrix employed (L= matrix L), K indicates the area weight of the fibre net in g/m<sup>2</sup>, X=bonded length ( $l$ ) in mm, Y=bonded width ( $b_l$ =75mm), and Z=specimen number. A total of 20 samples were tested.

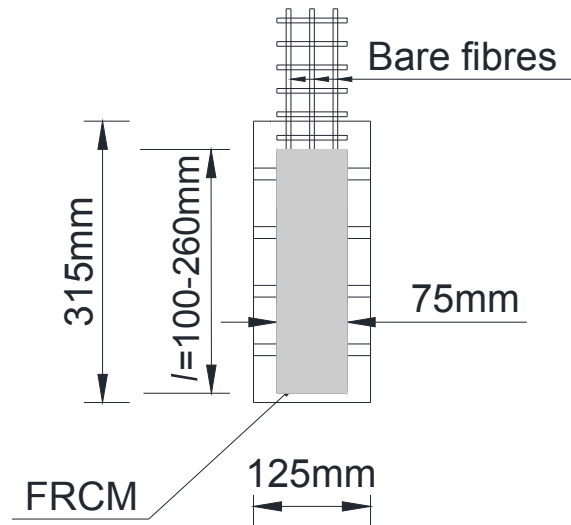


Figure 3: Specimens geometry.

The samples were located in a steel frame and restrained to avoid rotations and distortions as shown in Figure 4. The ends of the strips were glued between two aluminium plates to provide homogenous distribution of stress and avoid slippage phenomena at the clamps.

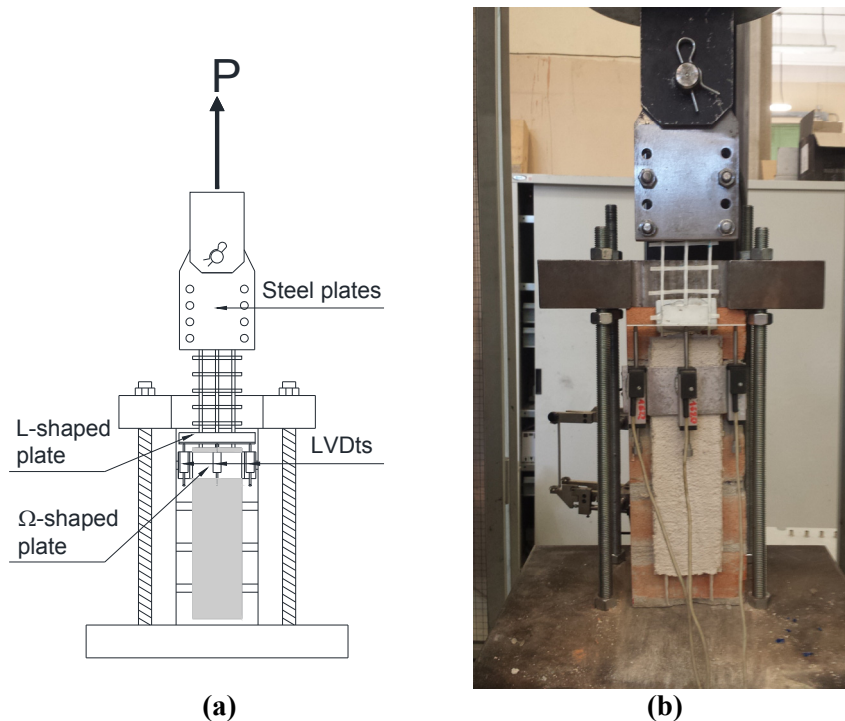


Figure 4: a) Single-lap direct-shear test set-up (measures in mm). b) Photo of specimen being tested

Two through-bolted steel plates connected to the testing machine through a hinge joint were used to clamp the aluminium plates. A  $\Omega$ -shaped aluminium plate was bonded to the masonry specimen near the loaded end of the composite. Two LVDTs were mounted on the sides of the  $\Omega$ -shaped plate to measure the displacement of the fibres with respect to the masonry support. The displacement measured by the central LVDT was used to control the test and was increased at a constant rate equal to 0.008 mm/s. The average displacement measured by the two LVDTs on the sides of the composite corresponds to the global slip  $g$  [14] if the substrate is considered rigid.

## 4 Experimental results

### 4.1 Basalt FRCM-masonry joints

Fifteen single-lap direct-shear tests were conducted on basalt FRCM-masonry joints, including three different bonded lengths, as explained before. Specimens failed at the matrix-fibre interface. However, two of them, namely MS\_BL350\_200\_75\_5 and MS\_BL350\_100\_75\_2, reported the failure of one of the external fibre bundles. This type of failure was attributed to the uneven distribution of the load among the three bundles.

In Table 2, the peak load  $P^*$  and the corresponding peak stress  $\sigma^*$  are reported for each specimen tested, with exception of samples MS\_BL350\_200\_75\_5 and MS\_BL350\_100\_75\_2.

Specimen Name	Peak Load (kN)	Average Peak Load (kN)	Peak Stress (MPa)	Average Peak Stress (MPa)	COV
MS_BL350_100_75_1	3.43	3.32	787.4	763.8	0.023
MS_BL350_100_75_3	3.34		767.1		
MS_BL350_100_75_4	3.26		749.0		
MS_BL350_100_75_5	3.27		751.6		
MS_BL350_200_75_1	4.77	4.57	1096.6	1051.3	0.053
MS_BL350_200_75_2	4.46		1025.5		
MS_BL350_200_75_3	4.78		1098.4		
MS_BL350_200_75_4	4.28		984.7		
MS_BL350_260_75_1	4.83	4.79	1110.4	1102.1	0.018
MS_BL350_260_75_2	4.72		1084.0		
MS_BL350_260_75_3	4.89		1125.1		
MS_BL350_260_75_4	4.72		1085.1		
MS_BL350_260_75_5	4.81		1105.8		

Table 2: Single-lap direct-shear tests for basalt FRCM

Equation (1) provides the expression for  $\sigma^*$ :

$$\sigma^* = P^*/(n \cdot A_b) \quad (1)$$

Where  $n$  is the number of longitudinal bundles within the bonded width and  $A_b$  is the area of a single bundle ( $1.45 \text{ mm}^2$ ).

The load responses of specimens with basalt FRCM composites are shown in Figure 5. Specimens with bonded length equal to 100 mm, 200 mm and 260 mm are reported in Figures 5a, 5b and 5c, respectively. Figure 5d allows for comparing the behaviour of all basalt FRCM specimens. The slope of the dashed line in this figure represents stiffness found for the single bundles tested in tension.

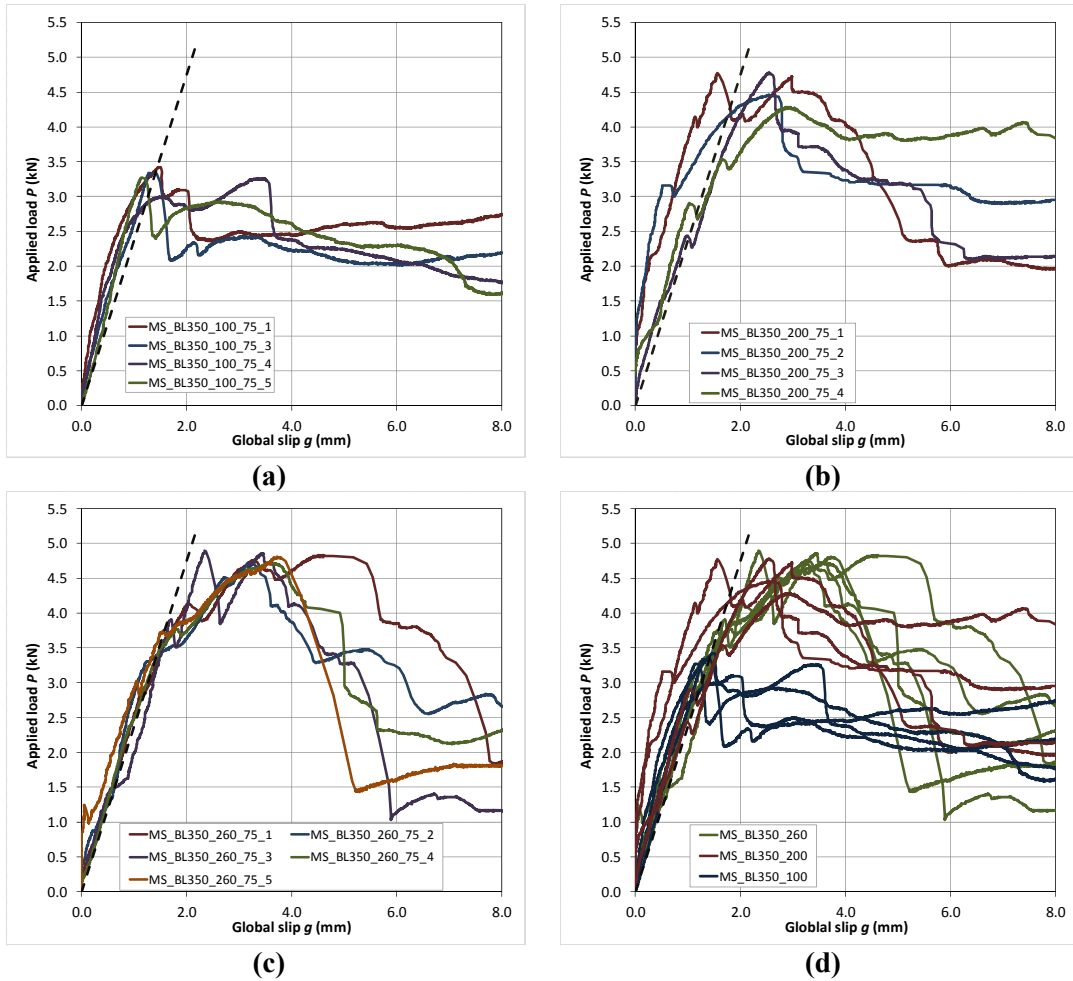


Figure 5: Applied load – global slip curves for specimens with basalt FRCM: a) bonded length  $\ell=100$  mm; b) bonded length  $\ell=200$  mm; c) bonded length  $\ell=260$  mm; d) All specimens

The failure was characterized by debonding of the fibre net from the embedding matrix and the presence of a crack near the loaded end (Figure 6a). This crack was located corresponding to the initial position of the first transversal bundle, as shown in (Figure 6b). This phenomenon may be related to the presence of stiff joints between longitudinal and transversal fibre bundles that determined stress

concentration just beyond the transversal bundles. Detachment of the matrix layer that covered the fibre between the crack and loaded end was observed in some cases. The peak load values obtained with single-lap tests are close to the measured fibre strength, indicating a good basalt fibre-matrix bond capacity.

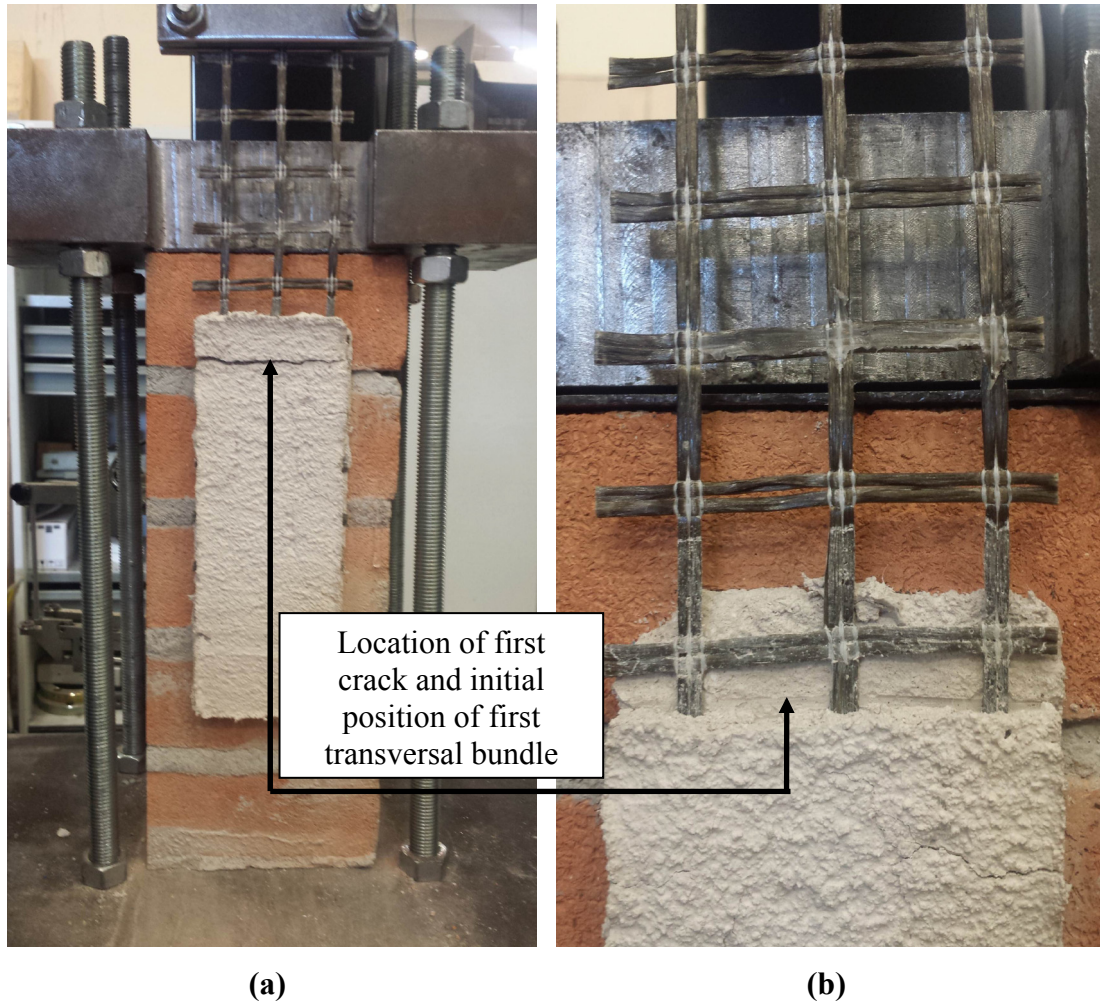


Figure 6: (a) Typical crack on tested basalt FRCM specimens. (b) Location of crack and initial position of the first transversal bundle

Results in Figure 5 and Table 2 indicate that the peak load  $P^*$  increases with bonded length  $l$  as reported in Figure 7. The peak load  $P^*$  for specimens with bonded length  $l=260$  mm is only slightly larger than the peak load for specimens with  $l=200$  mm (average increase = 4.8%). This suggests that the length needed to fully establish the stress transfer mechanism (i.e. the effective bonded length [11]) is less than 260 mm.

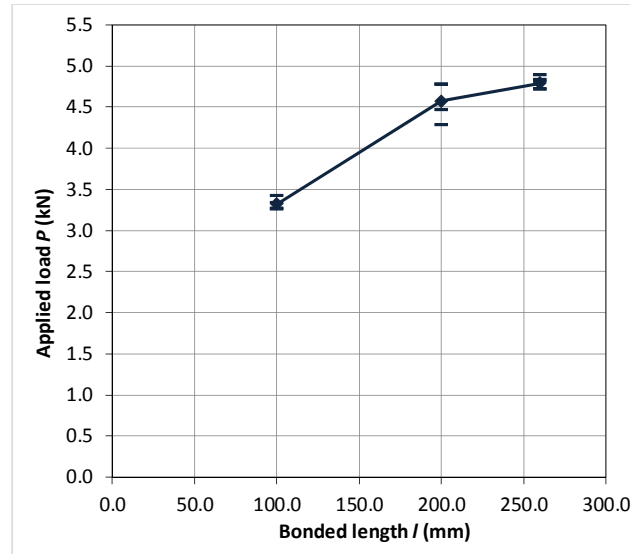


Figure 7: Variation of the peak load as a function of the bonded length for basalt FRCM

Regarding the shape of the curves, it is possible to identify a first linear branch that depends on the elastic behaviour of the matrix-fibre interface, as seen in Figure 5. As a matter of fact, for the specimens with  $l=100$  mm, the peak load is reached during this phase. For MS\_BM350\_75\_200 and MS\_BM350\_75\_260 series, this first branch is followed by a nonlinear one until they reach their respective peak loads. This behaviour is particularly evident for specimens with  $l=260$  mm. After the peak load is achieved, the applied load decreases with increasing global slip until attaining a constant value corresponding to the contribution of friction. This behaviour resembles the idealized curve shown in Figure 1.

## 4.2 Glass FRCM-masonry joints

Five single-lap direct-shear tests were conducted on glass FRCM-concrete joints with a bonded length  $l=260$  mm. In Table 3, for each specimen tested, the peak load  $P^*$  and the corresponding peak stress  $\sigma^*$  are reported.

Specimen Name	Peak Load (kN)	Mean Peak Load (kN)	Peak Stress (MPa)	Mean Peak Stress (MPa)	COV
MS_GL250_260_75_1	2.04	2.09	543.8	557.8	0.057
MS_GL250_260_75_2	1.94		516.5		
MS_GL250_260_75_3	2.23		593.9		
MS_GL250_260_75_4	2.07		552.7		
MS_GL250_260_75_5	2.18		582.0		

Table 3: Single-lap direct-shear tests for glass FRCM

The load responses of specimens with glass FRCM composites are reported in Figure 8. The slope of the dashed line in this figure represents the stiffness found for the single bundles tested in tension. As for the case of basalt samples, the response in this case starts with a linear elastic part, which depends on bond characteristics, followed by a nonlinear branch. Further tests will be carried out by the authors in order to establish the effective bonded length of glass FRCM-masonry joints.

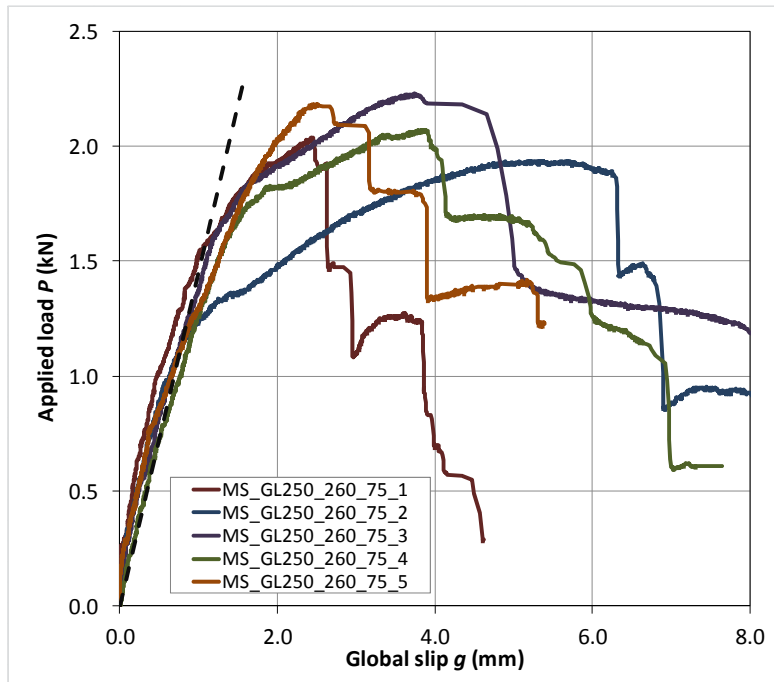


Figure 8: Applied load – global slip curves for specimens with glass FRCM

The glass FRCM specimens showed fibre debonding at the fibre-matrix interface. However, the increasing slip of the fibres within the embedding matrix was generally followed by rupture of one or more fibre bundles inside the matrix at or near the loaded end, as can be noted from sudden drops in the load responses. For glass fibres, cracks in the matrix were not observed.

## 4.2 Comparison of basalt and glass FRCM-masonry joints

Considering the ultimate tensile strength of the fibres, the peak loads attained with glass FRCM composites are lower than those attained with basalt FRCM composites with the same bonded length, as shown in Figure 9. It is also possible to clearly differentiate the initial larger stiffness of the basalt FRCM composites when compared to glass ones.

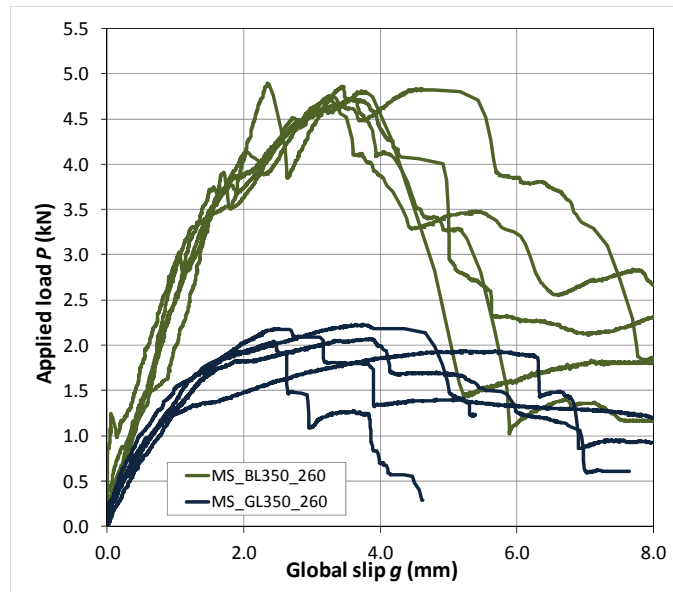


Figure 9: Comparison of applied load – global slip curves for specimens with basalt and glass FRCM-masonry joints with bonded length  $\ell=260$  mm

## 5 Sustainability of retrofit alternatives

In the last decades several studies have focused about the problem of retrofitting and strengthening existing buildings, mainly dealing with the mechanical and structural performances of the available alternatives. On the contrary, very few works have analysed the sustainability issues about these operations [15]. The most diffused and reliable method to assess the environmental impacts of a product is via a Life Cycle Assessment framework, in accordance to ISO standards 14040:2006 [16] and 14044:2006 [17]. This tool allows evaluating the environmental impact of strength and durability/service life related functional unit (FU) of reference over its entire life cycle, within determined system boundaries. Its application is fast growing up also to evaluate building materials sustainability [18].

In this work a LCA study has been used to assess the sustainability of the FRP and FRCM retrofitting/strengthening systems, and also to compare the influence of the type of fibres used on the overall environmental footprint of the products. The method is made by four mandatory phases: (1) the goal and scope definition phase, (2) the inventory analysis (LCI) phase, (3) the impact assessment (LCIA) phase, and (4) the interpretation phase. A cradle-to-gate approach has been used, i.e. from the extraction of the materials until the placement into the market of the product. The use of the product and the end-of-life stages are not included in the analysis, according to the system boundaries shown in Figure 10. The assessment has been made using OpenLCA 1.4.1 software [19], using a functional unit (FU) of  $1\text{ m}$  of retrofit intervention. It should be mentioned that, at this stage of the analysis, considerations about the overall retrofitting/strengthening capacities of the FRP and FRCM systems were not taken into account for the definition of the FU. The reference specimens selected for the study, and their main characteristics are

described in Table 4. Inventory data used were taken from the European Reference Life Cycle Database 3.0 (ELCD) [20] and from [21]. The allocation procedure is based on physical causation per unit of intervention, i.e. with mass allocation.

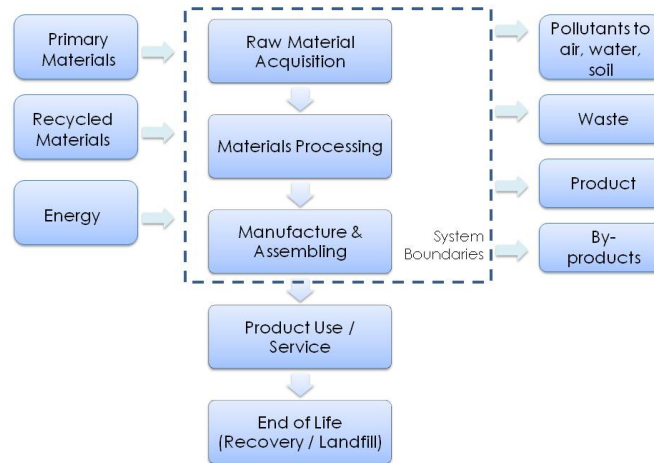


Figure 10: System boundaries for the LCA study, cradle-to-gate approach

System	$t$ (mm)	$b_f$ (mm)	Effective bonded length (mm)	Achieved load (N)	Area fibres (mm <sup>2</sup> )	$t$ fibre (mm)
	Epoxy-Resin					
BFRP	1	75	100	4365	4.35	0.29
GFRP	1	75	100	4098	3.75	0.25
	Cementitious Matrix					
BFRCM	10	75	260	4794	4.35	0.29
GFRCM	10	75	260	2093	3.75	0.25

Table 4: Reference specimens analysed (FU= 1m of intervention)

## 5.1 Analysis and results

The LCA results are presented in this section: a problem-oriented methodology has been chosen for the impact assessment. This approach involves the environmental impacts associated with eutrophication, acidification, human toxicity, eco-toxicity, etc., which impacts are quantified by proper characterisation factors, i.e. kg CO<sub>2</sub> eq. for global warming potential. Accordingly, the categories proposed by the CML 2002 method were used [22]. Results are listed in Table 5 for each alternative intervention analysed: the main comment that can be drawn is that the use of the epoxy resin is a dominating variable in affecting the environmental impacts of the solution. In fact, for almost all the environmental problems, the FRP system is responsible for higher impacts, even though the resin thickness is sensibly lower than the cementitious matrix, and hence less material is used in the FRP solution. Additionally, the use of basalt fibres instead of glass ones determines lower impacts for the majority of the categories.

			BFRP	GFRP	BFRCM	GFRM
DP	Abiotic Depletion	kg SB eq.	5.35E-03	5.35E-03	2.29E-09	3.90E-07
AP	Acidification Potential	kg SO <sub>2</sub> eq.	3.82E-03	3.84E-03	1.92E-04	2.10E-04
EP	Eutrophication Potential	kg PO <sub>4</sub> eq.	7.77E-04	6.53E-04	1.83E-04	5.95E-05
GWP	Global Warming Potential	kg CO <sub>2</sub> eq.	6.00E-01	6.00E-01	7.89E-03	8.52E-03
ODP	Ozone Layer Depletion Potential	kg CFC11 eq.	1.62E-09	6.06E-09	2.10E-09	6.53E-09
HTP	Human Toxicity Potential	kg 1.4DB eq.	4.60E-02	4.83E-02	7.63E-03	9.92E-03
FAETP	Freshwater Aquatic Ecotoxicity Potential	kg 1.4DB eq.	2.22E-02	2.22E-02	5.33E-04	5.42E-04
TETP	Terrestrial Ecotoxicity Potential	kg 1.4DB eq.	2.64E-03	2.66E-03	2.54E-05	4.99E-05

Table 5: LCA results

For the “glass fibre” product, similar data set alternatives are available in the inventory used during this work. Hence, a sensitivity analysis has been performed to evaluate the accuracy of the analysis: in particular, the equivalent material which can be potentially used are continuous filament glass fibres and glass wool as reported in ELCD database 3.0 [20]. As the in-depth description of the productive processes of the fibres is out of the scope of this work, the underlying details of this process are not covered in this paper. To observe the sensitivity of the two alternatives, the results are shown in Figure 11 for the GFRP system (FU = 1 m of intervention) in the GWP, EP, AP and ADP categories. On the contrary, for the “basalt fibre” product, this analysis could not be done due to the lack of reliable data. Results indicate that the two alternatives do not highly influence the overall impacts (maximum difference in the EP category = 8.9%).

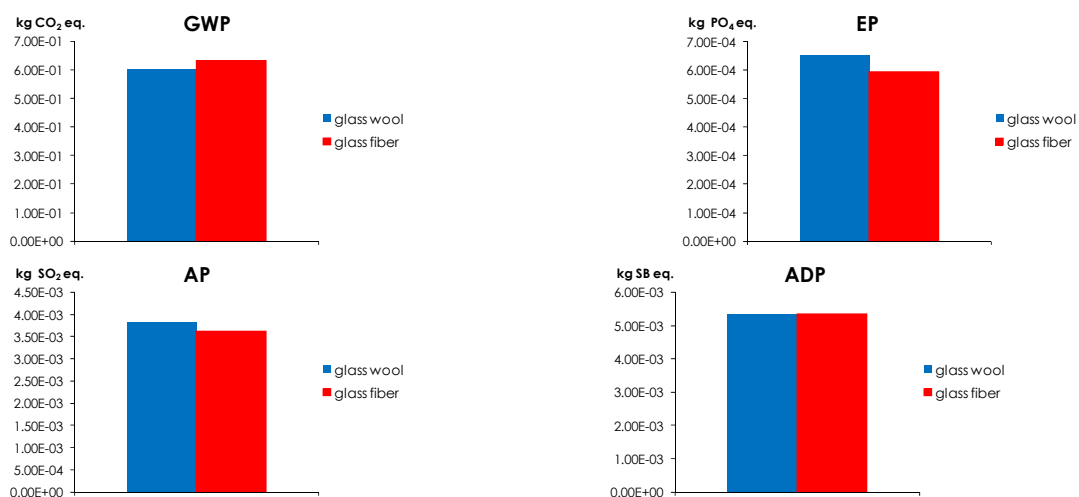


Figure 11: Sensitivity analysis results

## 5 Conclusions

The experimental results of 20 single-lap direct-shear FRCM-masonry joints with basalt and glass fibres were presented in this paper. Different bonded lengths were employed for basalt samples.

Basalt FRCM-masonry joints generally failed due to debonding of the fibre at the matrix-fibre interface. The peak load increased at different rates with increasing bonded length. However, the slight load increase (4.8%) between samples with bonded lengths of 200 and 260 mm suggests that the effective bonded length is lower than 260 mm.

It was possible to observe a crack located at the original position of the first transversal bundle, which was attributed to the stress concentration caused by the presence of stiff joints between longitudinal and transversal fibre bundles. The applied load-global slip curves resemble the idealized behaviour proposed by D'Antino et al [11] for PBO FRCM-concrete joints and confirmed for carbon and glass FRCM-concrete joints.

Glass FRCM-concrete joints also failed due to debonding of the fibre from the embedding matrix, although rupture of one or more fibre bundles was observed for some specimens. Glass FRCM composites reported peak load values lower than the basalt ones. Future tests are planned to determine the value of the effective bond length of glass FRCM-masonry joints.

Concerning the environmental impacts related to the FRCM intervention, the LCA study demonstrated its superior sustainability against FRP equivalent alternative. The use of basalt fibres determines also environmental gains in most of the analysed categories. However, additionally reliable inventory data about basalt fibres production are necessary to provide more accurate analyses for assess the proper influence of their application into strengthening/retrofitting systems.

## References

- [1] A. D'Ambrisi, L. Feo, F. Focacci, "Experimental and analytical investigation on bond between Carbon-FRCM materials and masonry", *Composites, Part B* 46, 15-20, 2013.
- [2] Y. Al-Salloum, M. Elsanadedy, S. Alsayed, Iqbal, R., "Experimental and numerical study for the shear strengthening of reinforced concrete beams using textile-reinforced mortar", *Journal of Composites for Constructions*, 74-90, 2012.
- [3] S. De Santis, G. de Felice, "Tensile behaviour of mortar-based composites for externally bonded reinforcement systems", *Composites, part B* 68, 401-413, 2015.
- [4] F.G. Carozzi, G. Milani, C. Poggi, "Mechanical properties and numerical modelling of Fabric Reinforced Cementitious Matrix (FRCM) systems for

- strengthening of masonry structures”, *Composites Structures*, 107, 711-725, 2014.
- [5] E. Grande, Imbimbo, M., Sacco, E., “Simple Model for Bond Behaviour of Masonry Elements Strengthened with FRP”, *Journal of Composites for Construction*, ASCE, May-June 2011.
- [6] F.G. Carozzi, C. Poggi, “Mechanical properties and debonding strength of Fabric Reinforced Cementitious Matrix (FRCM) systems for masonry strengthening”, *Composites: Part B* 70, 215-230, 2015.
- [7] J.F. Chen, J.G. Teng, “Anchorage strength models for FRP and steel plated bonded concrete”, *Journal of Structural Engineering*, 127(7), 784-191.
- [8] M.R. Valluzzi, “Round Robin Test for composite-to-brick shear bond characterization”, *Materials and Structures* 45:1761-1791, 2012.
- [9] C. Carloni, K.V. Subramaniam, “FRP-Masonry Debonding: Numerical and Experimental Study of the Role of Mortar Joints”, *Journal of Composites for Constructions*, Vol. 16, No. 5, 2012.
- [10] ACI Committee 549, “Guide to Design and Construction of Externally Bonded Fabric-Reinforced Cementitious Matrix (FRCM) Systems for Repair and Strengthening Concrete and Masonry Structures”, ACI549.4R-13, Farmington Hills, MI, U.S.A., 2013.
- [11] T. D’Antino, C. Carloni, C., L.H. Sneed, C. Pellegrino, “Matrix-fiber bond behavior in PBO FRCM composites: a fracture mechanics approach”, *Engineering Fracture Mechanics*, Vol. 117, pp. 94-111, 2013.
- [12] ASTM International, “Standard test method for tensile properties of polymer matrix composite materials”, ASTM D3039/D3039M-08, West Conshohocken, USA, 2008.
- [13] Comité Européen De Normalization, “Methods of test for mortar for masonry – Part 11: determination of flexural and compressive strength of hardened mortar”, UNI EN 1015-11, Brussels, Belgium, 2007.
- [14] K.V. Subramaniam, C. Carloni, L. Nobile, “Width effect in the interface fracture during debonding of FRP sheets from concrete”, *Engineering Fracture Mechanics*, Vol. 74, pp. 578-594, 2007.
- [15] L. Napolano, C. Menna, D. Asprone, A. Prota, G. Manfredi, “LCA-based study on structural retrofit options for masonry buildings”, *International Journal of Life Cycle Assessment* 20, 23-35, 2015.
- [16] ISO 14040, “Environmental management - Life cycle assessment - Principles and framework”, 2006.
- [17] ISO 14044, “Environmental management - Life cycle assessment - Requirements and guidelines”, 2006.
- [18] F. Faleschini, P. De Marzi, C. Pellegrino, “Recycled concrete containing EAF slag: environmental assessment through LCA”, *European Journal of Environmental and Civil Engineering* 18(9), 1009-1024.
- [19] GreenDELta, OpenLCA v. 1.4.1, 20 February 2015.
- [20] European Commission, European Reference Life Cycle Database 3.0 (ELCD), 2013, Joint Research Centre.

- [21] A.D. La Rosa, G. Cozzo, A. Latteri, G. Mancini, A. Recca, G. Cicala, “A Comparative Life Cycle Assessment of a Composite Component for Automotive”, *Chemical Engineering Transactions* 32, 1723-1728, 2013.
- [22] J.B. Guinée, M. Gorrée, R. Heijungs, G. Huppes, R. Kleijn, A. de Koning, L. van Oers, A. Wegener Sleeswijk, S. Suh, H.A. Udo de Haes, H. de Bruijn, R. van Duin, M.A.J. Huijbregts, “Handbook on life cycle assessment. Operational guide to the ISO standards. IIa: Guide. IIb: Operational annex”, Kluwer Academic Publishers, Dordrecht, 692 pp, 2002.